Electrically Active Tropical Cyclone Diurnal Pulses in the Atlantic Basin

SARAH D. DITCHEK, KRISTEN L. CORBOSIERO, ROBERT G. FOVELL, AND JOHN MOLINARI

Department of Atmospheric and Environmental Sciences, University at Albany, State University of New York, Albany, New York

(Manuscript received 29 April 2019, in final form 22 July 2019)

ABSTRACT

While the frequency and structure of Atlantic basin tropical cyclone diurnal cooling and warming pulses have recently been explored, how often diurnal pulses are associated with deep convection was left unanswered. Here, storm-relative, GridSat-B1, 6-h IR brightness temperature difference fields were supplemented with World Wide Lightning Location Network (WWLLN) data to answer that question. Electrically active, long-lived cooling and warming pulses were defined objectively by determining critical thresholds for the lightning flash density, areal coverage, and longevity within each pulse. Pulses with lightning occurred 61% of the time, with persistently electrically active pulses (≥9 h, ACT) occurring on 38% of pulse days and quasi–electrically active pulses (3–6 h, QUASI) occurring on 23% of pulse days. Electrically inactive pulses (<3 h, INACT) occurred 39% of the time. ACT pulse days had more pulses located right-of-shear, the preferred quadrant for outer-rainband lightning activity, and were associated with more favorable environmental conditions than INACT pulse days. Cooling pulses were more likely to occur in lower-shear environments while warming pulses were more likely to occur in high-shear environments. Finally, while the propagation speeds of ACT and INACT cooling pulses and ACT warming pulses did lend support to the recent gravity wave and tropical squall-line explanations of diurnal pulses, the INACT warming pulses did not and should be studied further.

1. Introduction

Dunion et al. (2014) took 6-h IR brightness temperature differences of North Atlantic major hurricanes from 2001 to 2010. In these difference fields, positive (negative) values indicated that warmer (cooler) cloud tops were present compared to 6 h prior. They found that most days had an area of cold cloud tops that propagated outward at around 5–10 $m\,s^{-1}$ over the course of the day. They defined this feature as a ''diurnal pulse'' and created a 24-h conceptual clock that identified at which radius the coldest cloud tops would be located based on local time (LT).

Generalizing and expanding the results of Dunion et al. (2014), Ditchek et al. (2019) created a climatology of diurnal pulses in the Atlantic basin for tropical cyclones of all intensities from 1982 to 2017. Pulses were defined objectively by determining critical thresholds for the magnitude of the IR differences and the areal coverage of cold cloud tops. The metric identified days with ''cooling pulses,'' similar to those documented by Dunion et al. (2014), and days without cooling pulses. For some of the days without cooling pulses, locally warm cloud tops that propagated outward at a similar speed as their cooling cloud top counterparts were discovered. These ''warming pulses,'' a previously undiscovered pulse type, were then also objectively defined using thresholds for the magnitude of the IR differences and areal coverage of warm cloud tops. Cooling and warming pulses were then divided into long-lived pulses and short-lived pulses based on their longevity. Therefore, each storm day (where each day begins at 0000 LT) was given a pulse-type classification: 1) long-lived cooling pulse (LLCP, 45.1% of the time), 2) short-lived cooling pulse (SLCP, 26.4% of the time), 3) long-lived warming pulse (LLWP, 8.5% of the time), 4) short-lived warming pulse (SLWP, 7.8% of the time), or 5) no pulse (NP, 12.2% of the time).

Ditchek et al. (2019) addressed many questions about cooling and warming pulses, including their frequency of occurrence overall, and within different intensity categories and shear groupings; their outward propagation speed; whether, and how, they are structurally influenced by shear; and, how the environment prior to pulse propagation differs between cooling and warming

Corresponding author: Sarah D. Ditchek, sarahditchek@gmail.com

DOI: 10.1175/MWR-D-19-0129.1

pulses. One of the questions left unanswered, however, was how often diurnal pulses are associated with deep convection.

Examples of diurnal pulses associated with deep convection have been previously documented in nature and in numerical modeling experiments. Using 85–91-GHz microwave satellite images, Dunion et al. (2014) showed that Emily (2005) and Felix (2007) had diurnal cooling pulses that were associated with cloud ice and, therefore, possibly deep convection (cloud ice is indicated by warm colors in their Figs. 1 and 2 and Figs. 4 and 5). Additionally, Dunion et al. (2019) used the highly realistic "hurricane nature run" of Nolan et al. (2013) to study diurnal cooling pulses and found that they were associated with enhanced vertical velocities and elevated total condensate, trailed by downdrafts and suppressed moisture, signatures of a cold pool. These findings led them to state that their results supported a tropical squall-line explanation of diurnal pulses.

IR brightness temperatures are useful for documenting the tropical cyclone diurnal cycle of inner-core deep convection and cirrus canopy oscillation (e.g., Browner et al. 1977; Muramatsu 1983; Steranka et al. 1984; Lajoie and Butterworth 1984; Kossin 2002; Wu and Ruan 2016; Knaff et al. 2019); alone, however, they are not ideal to detect deep convection outside of the inner core as they merely depict the temperature at the top of the cirrus canopy, which can obscure areas of deep convection. For example, the cold cloud tops might be an area of cirrus that was advected radially outward, not associated with deep convection. IR brightness temperatures and their associated differences, therefore, only identify the spatial location of a diurnal pulse, not whether it was associated with deep convection.

To determine whether a pulse was associated with deep convection, here, a 2005–17 subset[1] of the Ditchek et al. (2019) dataset was supplemented with data from the World Wide Lightning Location Network (WWLLN, section 2) to determine whether pulses were electrically active. As lightning has been found to occur in areas of 5–10 m s^{-1} updrafts (Zipser and Lutz 1994; Black and Hallett 1999; Deierling and Petersen 2008), it is not surprising that lightning has been found to be a sufficient, but not necessary, proxy for deep convection in tropical cyclones (Corbosiero and Molinari 2002, 2003; Abarca et al. 2011; Stevenson et al. 2016, 2018).

To identify whether pulses were electrically active, an objective metric was created (section 3). This metric identified long-lived cooling and warming pulses that were electrically active, quasi–electrically active, or electrically inactive based on thresholds for lightning flash density, lightning flash coverage, and longevity. The following questions are answered in section 4 for the electrically active and electrically inactive pulse types identified by the objective metric:

- How often are pulses electrically active?
- Do electrically active pulses have a preferred orientation with respect to the vertical wind shear?
- What is the 6-h IR brightness temperature evolution for days when an electrically active pulse did and did not occur?
- What, if any, is the difference in propagation speed between pulses that were, and were not, electrically active?
- Do electrically active pulses occur more frequently in storms of higher intensity?
- Is there a preferred shear environment in which electrically active pulses exist?
- Do days on which electrically active pulses occur have more favorable environments for deep convection?

A succinct comparison between electrically active pulse types, including answers to the above questions, is presented in section 5.

2. Data

The Ditchek et al. (2019) climatology incorporated: 1) four times daily, Atlantic-basin TC location and intensity data obtained from the Hurricane Database (HURDAT2; Landsea and Franklin 2013), interpolated to 3-h resolution, where storms included followed that of Ditchek et al. (2019) (storms of tropical depression or greater strength, storms that were not extratropical or subtropical, storm times with storm centers south of 40°N, and storm times before a storm made landfall for greater than 6 h); 2) Statistical Hurricane Intensity Prediction Scheme (SHIPS; DeMaria and Kaplan 1994, 1999; DeMaria et al. 2005) database p = 850–200-hPa, r = 0–500-km shear magnitude (kt) and direction (°), and SHIPS environmental fields for each storm time[2] that were linearly interpolated to 3-h temporal resolution, with SHIPS shear converted to meters per second (1 kt ~ 0.5144 m s^{-1}); and, 3) 3-h temporal resolution and 0.07° × 0.07° horizontal resolution GridSat-B1 IR brightness temperature data.

For each storm time, the IR brightness temperature data was extracted on a 600-km × 600-km storm-centered grid.

[1] This subset was taken since the first, complete, Atlantic basin tropical cyclone season monitored by WWLLN was 2005 (Rodger et al. 2009).

[2] For a description SHIPS environmental fields included, please see Ditchek et al. (2019).

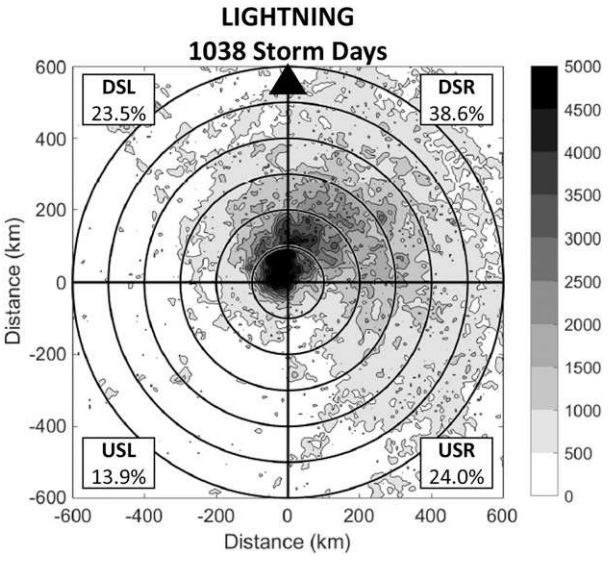

FIG. 1. A plan-view, shear-rotated, composite of the spatial location of all lightning flashes for all storm days. The shear vector points to the top of the plot (black triangle). Black range rings are overlaid every 100 km from r = 100–600 km. Black lines divide the figure into downshear-left (DSL), downshear-right (DSR), upshear-right (USR), and upshear-left (USL) quadrants. Percentages indicate the frequency of lightning flash occurrence in each quadrant.

For each storm, 6-h IR brightness temperature differences every 3 h were then calculated on the storm-centered, 0.07° × 0.07° resolution grid. Here, 6-h IR brightness temperature difference fields, HURDAT2 data, and SHIPS data over the 13-yr period of 2005–17 were retrieved from the Ditchek et al. (2019) climatology. This yielded 6787 6-h IR brightness temperature difference storm-relative grids over 1038 storm days that encompassed 196 individual storms, a 61% decrease in sample size from Ditchek et al. (2019). Qualitatively similar results to those in Ditchek et al. (2019) were found using the 2005–17 subset, despite the reduction in sample size.

Lightning flash locations ±1.5 h of each storm time were obtained from the WWLLN and binned to a storm-relative, 0.07° × 0.07° grid, matching the GridSat-B1 resolution. The 2005–14 North Atlantic basin adjustment factors used in Stevenson et al. (2018) and the 2015–17 adjustment factors of 3.3, 3.4, and 3.6 calculated using the same method as in Stevenson et al. (2018) (S. N. Stevenson 2019, personal communication) were then applied to the WWLLN data. The adjustment factors account for the increase in sensors and improved detection algorithms, and, therefore, detection efficiency over time, enabling the yearly WWLLN lightning density to match the lightning density climatology of the spaceborne Optical Transient Detector (OTD) and the Lightning Imaging Sensor (LIS) on board the Tropical Rainfall Measuring Mission's (TRMM) satellite (Rodger et al. 2009; Abarca et al. 2010; DeMaria et al. 2012; Stevenson et al. 2018).

TABLE 1. The number and percentage of days with each pulse type (column 2) and the percentage of total lightning that occurred on each pulse-type day (column 3).

Pulse type	No. (%)	Pulse day lightning (%)
LLCP	456 (43.9%)	61.5%
SLCP	281 (27.1%)	22.6%
LLWP	97 (9.3%)	9.2%
SLWP	81 (7.8%)	2.4%
NP	123 (11.9%)	4.3%
All	1038 (100%)	100%

The 6-h IR brightness temperature differences and lightning flash location storm-relative grids were then rotated so that the shear vector was pointing due north. Results in this paper are examined in this shear-rotated coordinate system.

3. Lightning distribution

Figure 1 depicts the distribution of lightning that occurred over all 1038 storm days.[3] In the inner core (r < 100 km), lightning flash count peaked in the downshear-left quadrant, while in the outer-rainband region (r > 200 km), lightning flash count peaked in the downshear-right quadrant. These results corroborate those found in Corbosiero and Molinari (2002, 2003) and, more recently, Stevenson et al. (2016).

Using the objective metric developed in Ditchek et al. (2019), each of the 1038 storm days were categorized as a day that had either a LLCP, SLCP, LLWP, SLWP, or NP. The number and percentage of days with each pulse type is given in column 2 of Table 1. Table 1 also includes the percentage of total lightning that occurred on each pulse-type day in column 3. Lightning occurred most frequently on cooling-pulse days (84.1% of the total lightning) and occurred least frequently on NP days (4.3% of the total lightning). This result is not surprising since cooling pulses are associated with colder cloud tops, which are a necessary (but not sufficient) indication for deep convection and, therefore, lightning. The percentage does not indicate, however, that the cooling pulses themselves were associated with deep convection. Rather, the percentage indicates that the environment on cooling-pulse days was overall more electrified than

[3] The average shear across all storm days was 8.1 m s^{-1} from the west-northwest.

the environment on warming-pulse and no-pulse days. The next section will detail the objective metric generated to determine whether the pulse itself was associated with lightning.

4. Objective electrically active diurnal pulse identification

To determine whether a pulse was electrically active, three criteria needed to be satisfied. First, for all long-lived and short-lived pulse day types, the lightning flash density within the pulse itself was calculated by

$$\frac{\sum L_P}{\text{area}_P}, \tag{1}$$

where L_P is the number of lightning flashes within P, the specific pulse type (i.e., LLCP, SLCP, LLWP, or SLWP) identified following the procedure detailed in Ditchek et al. (2019), and area_P is the area covered by the identified pulse. To calculate the area of the pulse, the number of grid boxes that had an identified pulse was multiplied by the area of the 0.07° × 0.07° grid box. Cooling- and warming-pulse storm times that had pulse flash densities that fell in the upper half of the distribution [>8.2 flashes $(100\,\text{km})^{-2}$] were identified.

To be sure that the metric did not favor a storm time where there was a large lightning flash count in a confined area, the area covered by lightning flashes within all long-lived and short-lived pulse day types was calculated by

$$\frac{\text{area}_L}{\text{area}_P}, \tag{2}$$

where area_L is the area covered by the lightning and area_P is as before. Since the lightning was binned to a 0.07° × 0.07° grid (section 2), calculating the area covered by the lightning was done similarly to calculating the area encompassed by the pulse. Cooling- and warming-pulse storm times with pulse flash coverages that fell in the upper half of that distribution (>0.56%) were identified.

Third, the number of hours in a given day where the lightning flash density and coverage criteria were satisfied was calculated. On a given day, if storm times that satisfied both the pulse flash density and coverage criteria existed for ≥9 h, that day was categorized as having an electrically active (ACT) pulse. If storm times that satisfied both the pulse flash density and coverage criteria existed for t = 3–6 h, that day was categorized as a day having a quasi–electrically active (QUASI) pulse. Days that had storm times that did not satisfy both pulse flash criteria or had storm times that satisfied both pulse flash criteria but existed for less than 3 h were characterized as electrically inactive (INACT) pulse days.

TABLE 2. The number and percentage of electrically active (ACT), quasi–electrically active (QUASI), and electrically inactive (INACT) pulse days for each long-lived pulse type and overall.

Pulse type (No.)	ACT	QUASI	INACT
Cooling pulse (456)	200 (43.9%)	110 (24.1%)	146 (32.0%)
Warming pulse (97)	10 (10.3%)	18 (18.6%)	69 (71.1%)
Total (553)	210 (38.0%)	128 (23.1%)	215 (38.9%)

As in Ditchek et al. (2019), hereafter, only days with long-lived pulses will be discussed, as long-lived pulses persisted over a longer period of the day and are the more frequent diurnal pulse type compared to short-lived pulses. Additionally, the descriptor long-lived will no longer be used, for brevity.

The number and percentage of ACT, QUASI, and INACT pulse days for cooling and warming pulses are given in Table 2. Overall, 38.0% of pulse days were ACT while 38.9% of pulse days were INACT. Cooling pulses were more likely to be ACT (43.9% of the time) while warming pulses were mostly INACT (71.1% of the time).

The objective metric successfully separated those pulse days that were electrically active from those that were not.[4] Figures 2a–c and 2g–i depict the number of pulses at a given location for cooling and warming pulses, respectively, and Figs. 2d–f and 2j–l show the summed lightning present in the cooling and warming pulses, respectively, for ACT, QUASI, and INACT days. The summed lightning for the ACT cooling pulses (Fig. 2d) depicts a lightning distribution that is similar to Fig. 1: an inner-core lightning peak in the downshear-left quadrant and an outer-rainband lightning peak in the downshear-right quadrant. The QUASI and INACT cooling pulses had much fewer and near zero lightning flashes, respectively (Figs. 2e,f). The lightning distribution for the (quite rare) ACT warming pulse (Fig. 2j) has a downshear-right maximum in the outer-rainband region, similar to Fig. 1, while the QUASI and INACT warming pulses had much less and near zero lightning flashes, respectively (Figs. 2k–i).

Since QUASI days had much less lightning than ACT days, the remainder of the paper will focus on ACT and INACT cooling and warming pulses.

[4] Using the upper quartile of the lightning flash density and coverage criteria did not separate pulse days that were ACT or QUASI from those that were INACT, as using that threshold included many ACT and QUASI days in the INACT category.

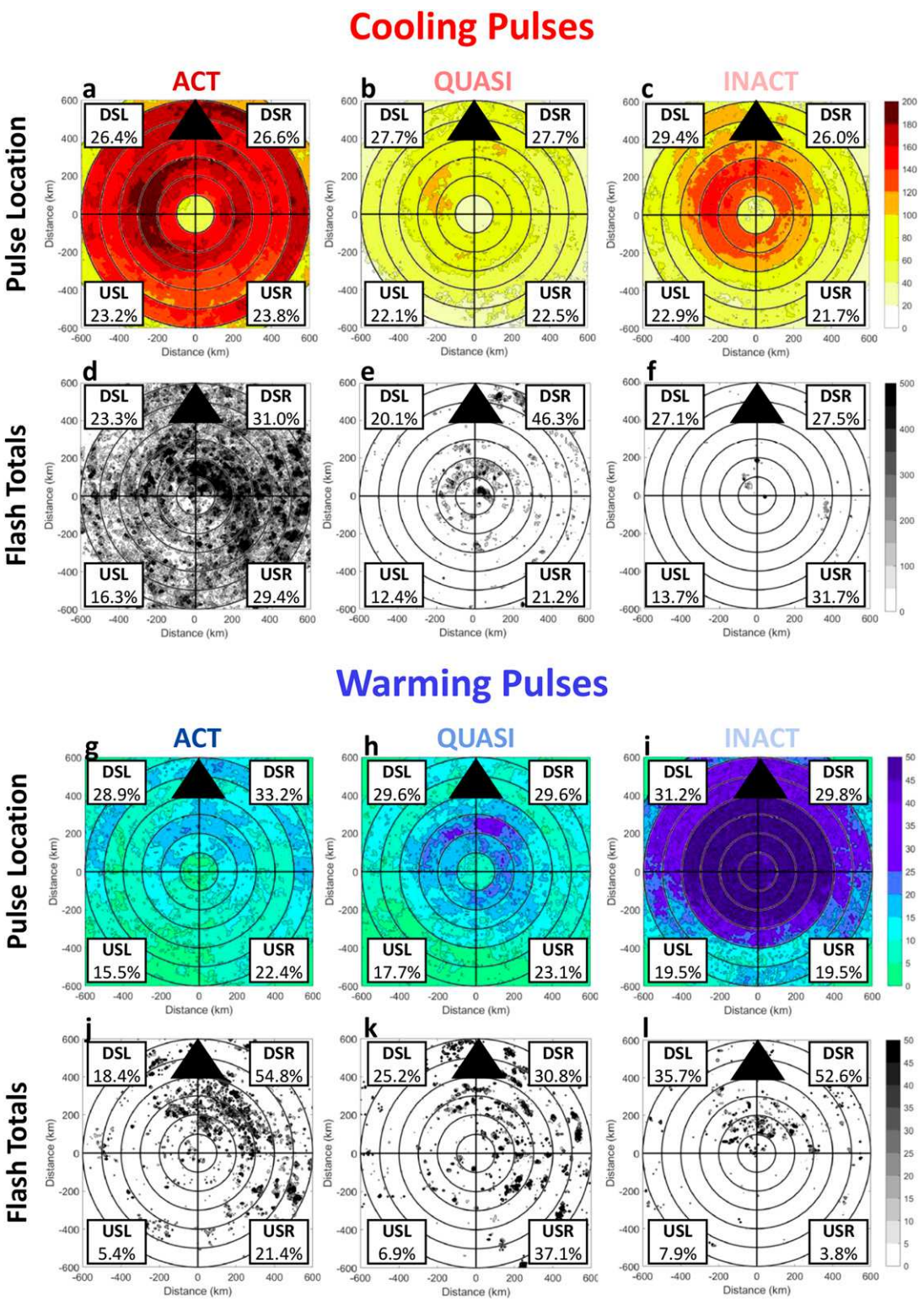

FIG. 2. A plan-view composite of (a)–(c),(g)–(i) the number of pulses at a given location and (d)–(f),(j)–(l) summed lightning in the pulses for (left) electrically active days (ACT), (middle) quasi–electrically active days (QUASI), and (right) electrically inactive days (INACT). The shear vector points to the top of each plot (black triangle). Black range rings are overlaid on each image every 100 km from $r = 100$–600 km. Black lines divide the figures into downshear-left (DSL), downshear-right (DSR), upshear-right (USR), and upshear-left (USL) quadrants. Percentages indicate the frequency of pulse location and lightning flash occurrence in each quadrant.

5. Results

a. Structural evolution

The 6-h IR composite brightness temperature difference evolutions with overlaid lightning for cooling and warming pulses that were ACT and INACT every 3 h from 0000 to 2100 LT are given in Figs. 3–6. Overlaid on each plan-view plot are black range rings every 100 km with the white range rings corresponding to the expected timing of the observed TC diurnal pulse using the extended version of the Dunion et al. (2014) diurnal clock (Ditchek et al. 2019, Fig. 2b).

For ACT cooling pulses, lightning was present in the inner core and at $r > 500$ km over the entire day (Fig. 3). Beginning at 0300 LT, the cooling pulse (decreasing cloud top temperatures, green to red shading) was located between the 0- and 200-km radii, and was associated with particularly enhanced lightning compared to outer radii and to 0000 LT. As the cooling pulse propagated outward from 0600 to 1800 LT, so too did the lightning, peaking primarily to the right of the shear vector as seen in Fig. 2d. In comparison, there was no coupled lightning associated with the outward-propagating INACT cooling pulse (Fig. 4). The INACT cooling pulse propagated outward primarily to the left of the shear vector, where lightning is less frequently observed outside of the core (Fig. 1).

Since warming pulses only occurred 9.3% of the time (Table 1, line 3, column 2), dividing this already small sample further yielded only 10 ACT warming-pulse days and 69 INACT warming-pulse days. As seen in Fig. 5, there was lightning present on the outer edge of the warming pulse itself, which is why these warming pulses were identified as ACT warming pulses. This lightning, however, was associated with the inner edge of a large swath of lightning associated with a highly convective, cooling pulse that propagated outward ahead of the warming pulse. This cooling pulse was "off-the-clock" in that it did not follow the Dunion et al. (2014) diurnal clock schematic. Only ACT warming-pulse days had an off-the-clock cooling pulse, however. As seen in Fig. 6, there is a weak signature of an off-the-clock, short-lived cooling pulse from 0300 to 0600 LT, but, otherwise, INACT warming pulses were not associated with an off-the-clock cooling pulse.

An off-the-clock cooling pulse was not seen in the Ditchek et al. (2019) composite of warming pulses from 1982 to 2017 (their Fig. 5). This is not surprising since ACT warming pulses occurred infrequently compared to INACT warming pulses in the 2005–17 subset presented here (10.3% of the time compared to 71.1% of the time; Table 2, line 2, columns 1 and 3). With INACT warming pulses occurring more frequently, the off-the-clock cooling pulse was likely averaged out in the larger sample used in Ditchek et al. (2019). Therefore, to understand why ACT warming-pulse days have pulses that do not follow the Dunion et al. (2014) diurnal clock schematic, case studies of days with ACT warming pulses should be an area of future research.

Similar spatial patterns to those in Figs. 3–6 were found for the spatial evolution of 6-h IR composite brightness temperature differences with overlaid lightning for TC days with similar intensities and similar shear values (not shown).

b. Axisymmetric framework

To calculate the propagation speed of the diurnal pulses and lightning seen in Figs. 3–6, azimuthal averages of the 6-h IR brightness temperature differences and the lightning flashes on days where ACT and INACT cooling and warming pulses occurred were computed using a 0.07° bin size, matching the GridSat-B1 resolution, sorted into bins centered on the hour, and averaged. Fourier harmonic analysis was then applied at each radius by fitting a series of sines and cosines to the data through least squares regression analysis following Ditchek et al. (2019). The azimuthally averaged diurnal harmonics of the 6-h IR brightness temperature difference for ACT and INACT cooling and warming pulses are depicted in Figs. 7a,b and 7e,f. Figures 7c,d and 7g,h depict the corresponding lightning flash evolution diurnal harmonics plus the mean lightning flash count at each radius over all hours so that nonnegative lightning counts would be shown. Propagation speeds were then calculated between 200 and 300 km and between 300 and 600 km, using the azimuthally averaged diurnal harmonics, and are given in Table 3.

1) Structure

Outward propagating cooling pulses were present in both 6-h IR brightness temperature difference azimuthal averages (Figs. 7a,b), with only the ACT cooling pulse having an associated outward propagating lightning signature, beginning around the 300-km radius (Figs. 7c,d). Additionally, ACT cooling pulses had larger diurnal amplitude and began propagating outward slightly earlier in the day than INACT cooling pulses.

Outward propagating warming pulses were present in both 6-h IR brightness temperature difference azimuthal averages (Figs. 7e,f), with only the ACT warming pulse having an associated outward propagating lightning signature, associated with an off-the-clock cooling pulse that propagated outward ahead of the warming pulse, beginning around the 300-km radius (Figs. 7g,h). This off-the-clock cooling pulse was not

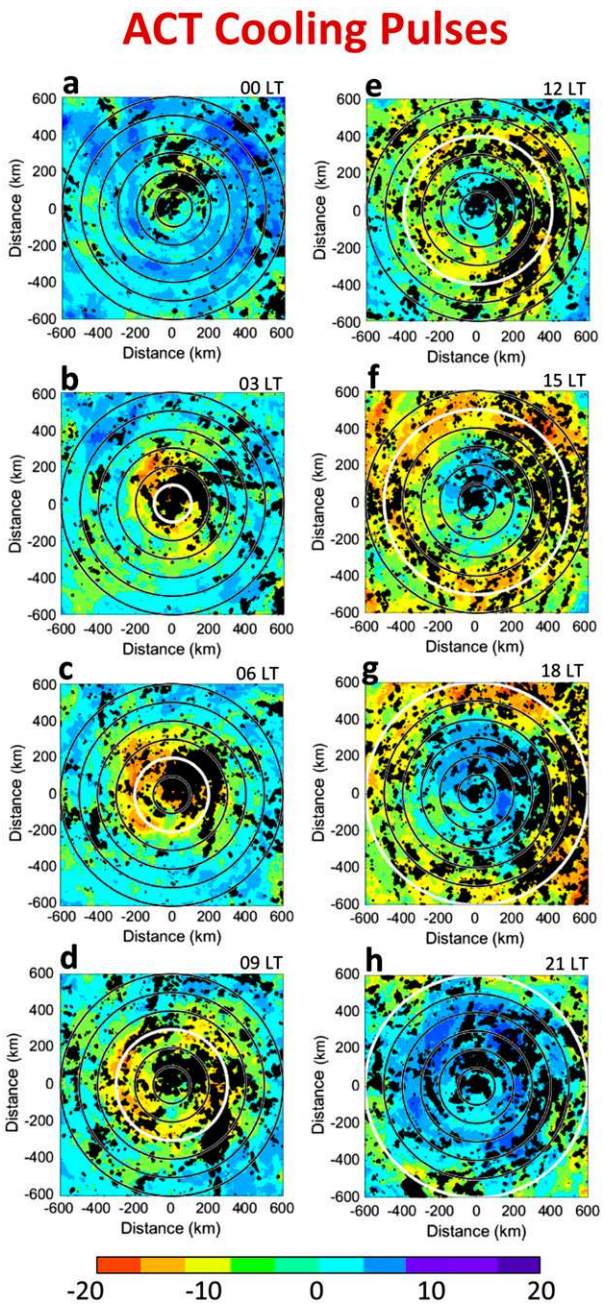

FIG. 3. A plan view of composite 6-h IR brightness temperature difference fields (K) ending at (a) 0000, (b) 0300, (c) 0600, (d) 0900, (e) 1200, (f) 1500, (g) 1800, and (h) 2100 LT with overlaid composite lightning ±1.5 h centered on the image ending time for days when electrically active (ACT) cooling pulses occurred. Lightning is filled for composite values of 0.25 and larger, for aesthetic purposes. The shear vector points to the top of each plot. Black range rings are overlaid on each image every 100 km from r = 100 to 600 km. White range rings indicate the radius at which the pulse should occur using the extended version of the Dunion et al. (2014) diurnal clock (Ditchek et al. 2019, Fig. 2b).

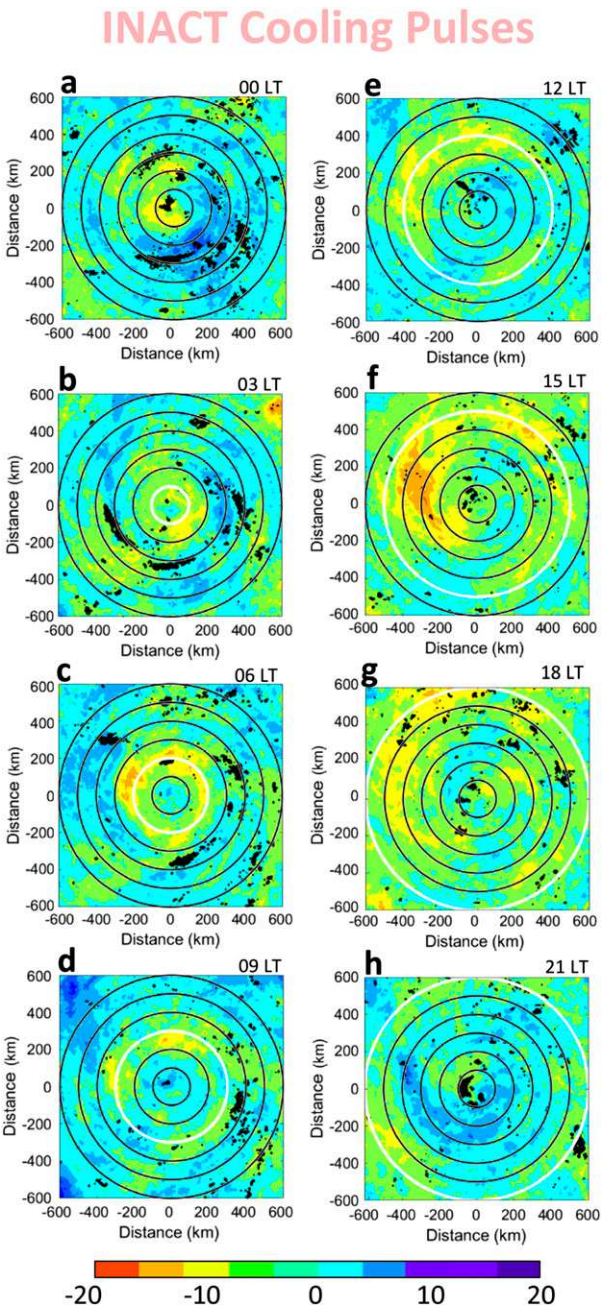

FIG. 4. As in Fig. 3, but for days when electrically inactive (INACT) cooling pulses occurred.

found to have propagated outward from inner radii the day prior to ACT warming-pulse days (not shown), implying that the dynamics that govern the off-the-clock pulse and associated ACT warming pulse at outer radii seen Fig. 7e might be different than those that govern the on-the-clock ACT cooling pulses seen in Fig. 7a. Additionally, as found in Ditchek et al. (2019), the structure of the warming-pulse harmonics were

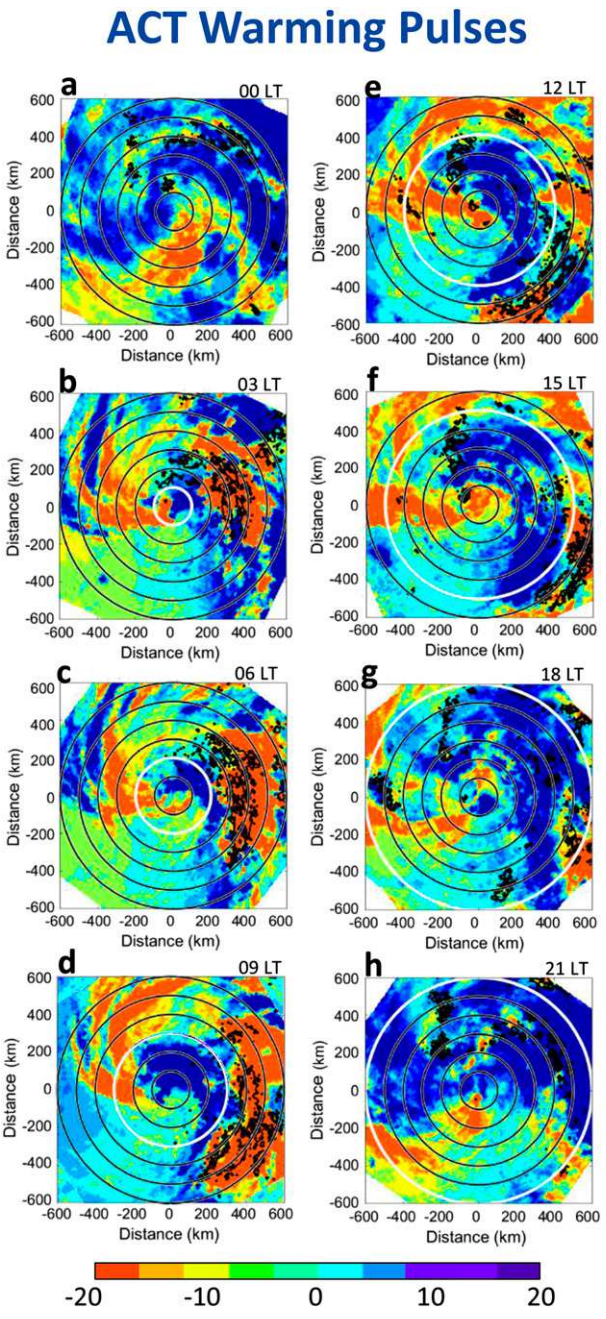

FIG. 5. As in Fig. 3, but for days when electrically active (ACT) warming pulses occurred.

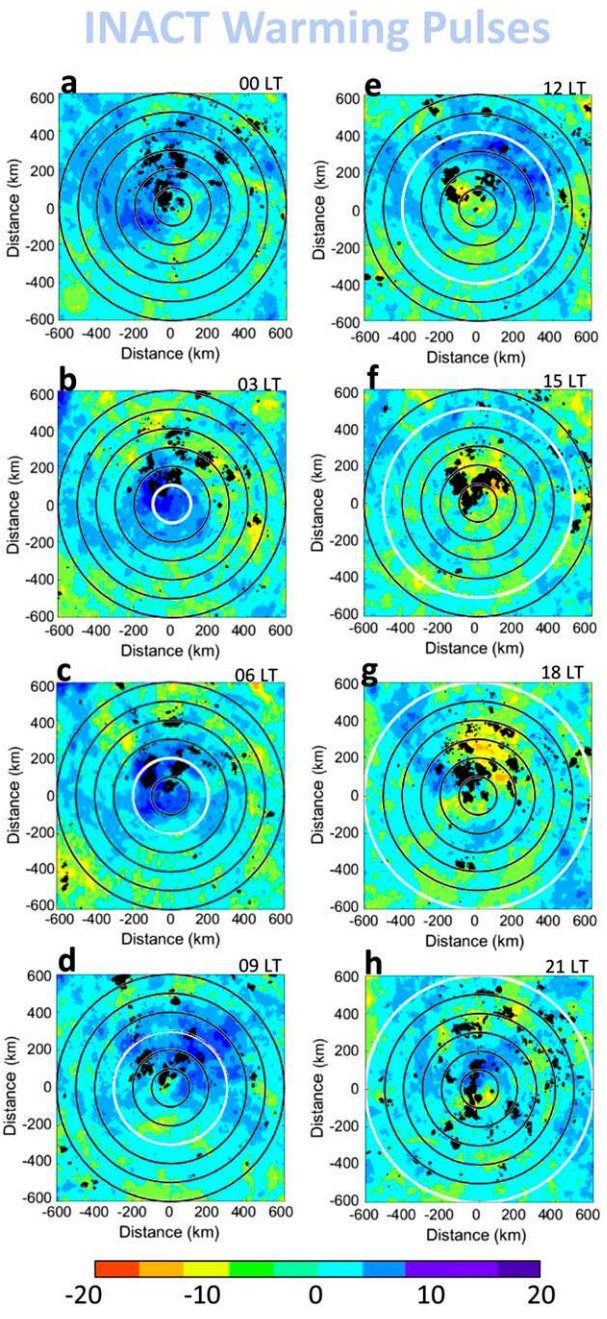

FIG. 6. As in Fig. 3, but for days when electrically inactive (INACT) warming pulses occurred.

different from the cooling-pulse harmonics in that the warming-pulse harmonics had larger amplitudes at inner radii.

2) PROPAGATION SPEED

Due to their ring-like nature, one of the Dunion et al. (2014) hypotheses for diurnal pulse propagation was that they might be governed by gravity waves dynamics, perhaps initiated from enhanced deep convection in the inner core. A gravity wave interpretation of diurnal pulses has also been suggested in recent research (Navarro et al. 2017; O'Neill et al. 2017; Ruppert and O'Neill 2019; Evans and Nolan 2019), with calculated gravity wave phase speeds similar to the diurnal pulse propagation speed of 5–10 m s^{-1} found in Dunion et al. (2014) and 8–14 m s^{-1} found in Ditchek et al. (2019).

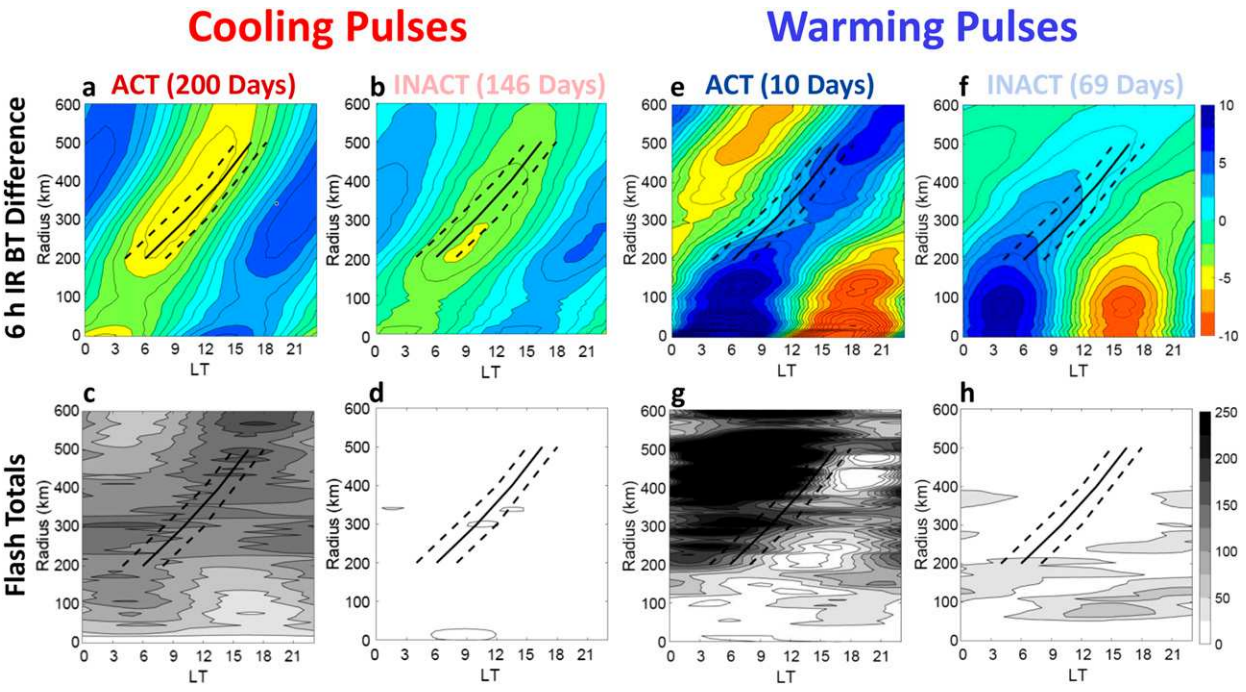

FIG. 7. Azimuthally averaged (a),(b),(e),(f) diurnal harmonics for the 6-h IR brightness temperature differences and (c),(d),(g),(h) diurnal harmonics plus the mean at each radius over all hours for summed lightning in the pulse for (a),(c),(e),(g) electrically active (ACT) and (b),(d),(f),(h) electrically inactive (INACT) cooling and warming pulses. Black lines correspond to the mean (solid), earliest (dashed), and latest (dashed) times of the onset of the diurnal pulse according to the original diurnal clock in Dunion et al. (2014).

The finding that diurnal pulses are a nearly ubiquitous feature of tropical cyclones may support this gravity wave interpretation as well (Ditchek et al. 2019). Results in Dunion et al. (2019) also supported a gravity wave interpretation of diurnal pulses, as they speculated that a gravity wave could provide the lift necessary for a tropical squall line to initiate.

Since theory dictates that convectively coupled waves often move slower than their counterparts, in other words, the waves remain waves but are slowed by latent heat release (Wheeler and Kiladis 1999; Dias and Pauluis 2009), if the diurnal pulse is a gravity wave, then ACT pulses should have a slower propagation speed than INACT pulses, as ACT pulses are associated with lightning, and, therefore, likely associated with deep convection. While INACT cooling pulses could either be associated with convection that is not electrified or a shallow-cirrus layer, INACT warming pulses are most certainly not associated with convection. They, therefore, should have the fastest propagation speed compared to the ACT pulses and the INACT cooling pulse. Complicating the interpretation of pulse propagation speeds is that at outer radii, diurnal pulses can be associated with cold pools (Dunion et al. 2019). This cold pool could act to increase the propagation speed of diurnal pulses at outer radii.

The propagation speed of the ACT cooling and warming pulses and the INACT cooling pulses increased with radius, likely due to an associated cold pool which would lend support to the Dunion et al. (2019) result that pulses take on tropical squall-line characteristics after propagating away from the inner core. Additionally, consistent with the convectively coupled wave theory, the ACT cooling and warming pulses had slower propagation speeds than the INACT cooling pulse between 300 and 600 km.

The tropical squall-line interpretation of diurnal pulses, however, does not apply to INACT warming pulses as they were most certainly not associated with convection and they were not associated with an off-the-clock cooling pulse. Therefore, it was not surprising that their propagation speed did not increase with radius, as there would be no associated cold pool. It was surprising,

TABLE 3. The propagation speed ($m\,s^{-1}$) of ACT and INACT cooling and warming pulses between 200 and 300 km and between 300 and 600 km.

	Cooling pulse		Warming pulse	
Radius	ACT	INACT	ACT	INACT
200–300 km	11.1	7.4	5.1	7.9
300–600 km	13.9	17.5	10.4	6.7

however, that INACT warming pulses had the slowest propagation speed despite not being associated with convection. This indicates that the gravity wave interpretation of diurnal pulses probably does not apply to INACT warming pulses. Since pulses are nearly ubiquitous in tropical cyclones (Ditchek et al. 2019), in order to create a unifying theory of diurnal pulses, the reason behind the existence of warming pulses needs to be determined. Therefore, observational and numerical modeling cases studies of diurnal pulses, specifically INACT warming pulses, should be conducted.

c. *Frequency*

Figure 8a depicts how frequently ACT and INACT cooling and warming pulses were detected within each intensity category, where intensity was taken as the maximum value reached on a given day. Days where major hurricane intensity was reached were dominated by ACT cooling pulses (dark red bars). On days when minor hurricane, tropical storm, and tropical depression intensity was reached, the frequencies of ACT cooling-pulse occurrence were similar. INACT cooling pulses (light red bars) occurred less frequently than ACT cooling pulses on days where major hurricane, tropical storm, and tropical depression intensity was reached. On days where minor hurricanes intensity was reached, however, INACT cooling pulses occurred slightly more often than ACT cooling pulses. Of all of the pulse categories, ACT warming pulses (dark blue bars) occurred least often (only 10 days, Table 2), and never on days of tropical depression intensity. Finally, INACT warming pulses (light blue bars) occurred most often on days that were tropical storm intensity and occurred least often on days of major hurricane intensity.

The influence of vertical wind shear on ACT and INACT cooling- and warming-pulse frequency is given in Fig. 8b, where shear was measured as the average magnitude on a given day. As in Ditchek et al. (2019), shear groupings were defined from the 1982–2017 shear distribution as low shear (lower quartile, $<4.4\,\mathrm{m\,s^{-1}}$), moderate shear (interquartile range, 4.4–10.6 $\mathrm{m\,s^{-1}}$), and high shear (upper quartile, $>10.6\,\mathrm{m\,s^{-1}}$). ACT cooling pulses dominated days that had moderate-shear environments. On days with low and high shear, however, the number of ACT and INACT cooling pulses were similar. ACT warming pulses never occurred in low-shear environments and INACT warming pulses dominated high-shear days. Overall, storms in lower- (higher-) shear environments were more likely to have cooling (warming) pulses.

A distinguishing feature of the ACT warming pulse is an associated off-the-clock cooling pulse (Figs. 5 and 7e). Since ACT warming-pulse days were found to occur in high-shear environments, it is certainly possible that

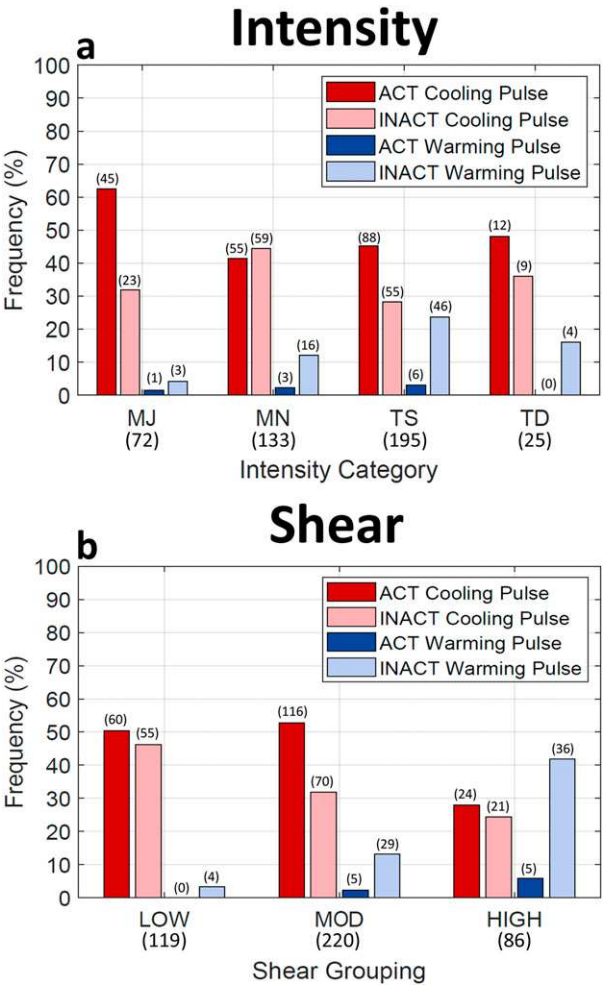

FIG. 8. Bar charts depicting the frequency (%) of electrically active (ACT) and electrically inactive (INACT) cooling pulses (dark and light red bars, respectively) and warming pulses (dark and light blue bars, respectively) (a) for each intensity category [major hurricane (MJ), minor hurricane (MN), tropical storm (TS), and tropical depression (TD)] and (b) for each shear grouping (low, moderate, and high). Values in parentheses represent the actual number of events that occurred.

high shear could be offsetting the cooling pulse and the observed ACT warming pulse is the trailing warming response amplified by daytime solar heating. The existence of the INACT warming pulse, however, complicates this interpretation, as INACT warming pulses were also found to occur in high-shear environments but were not found to be associated with an off-the-clock cooling pulse, at least in a composite sense. Case studies of ACT and INACT warming pulses should be conducted to further understand the nature of these warming pulses.

d. *Differences between ACT and INACT days*

To quantify the difference in cloud-top temperatures between ACT and INACT cooling and warming pulse

TABLE 4. The mean and standard deviation of variables on electrically active (ACT) cooling-pulse, electrically inactive (INACT) cooling-pulse, ACT warming-pulse, and INACT warming-pulse days. Significant differences between cooling-pulse days and warming-pulse days are calculated at the 99% confidence level assuming both equal and then unequal variances using a Student's *t* test. Variables that are statistically different are indicated by boldface text.

Variable	Units	Radius	Pressure	Cooling pulse		Warming pulse	
				ACT	INACT	ACT	INACT
IR	K	r = 0–600 km	—	**261.0 ± 29.7**	**267.2 ± 26.5**	**256.7 ± 30.2**	**274.0 ± 24.4**
Intensity	kt	—	—	65.6 ± 32.8	65.1 ± 26.8	**58.6 ± 15.9**	**49.4 ± 17.6**
MPI	kt	—	—	**141.4 ± 16.7**	**126.1 ± 22.4**	**142.9 ± 18.6**	**114.3 ± 26.7**
Daily SST	°C	r = 0–50 km	—	**28.5 ± 1.0**	**27.4 ± 1.5**	**28.0 ± 1.1**	**26.6 ± 1.5**
OHC	kJ cm^{-2}	—	—	**58.6 ± 29.8**	**36.6 ± 29.0**	**44.9 ± 33.5**	**24.9 ± 19.9**
TPW	mm	r = 0–500 km	—	**56.0 ± 5.0**	**54.1 ± 5.6**	**55.3 ± 4.4**	**49.2 ± 5.4**
Θ_e	K	r = 200–800 km	p = 1000 hPa	**351.5 ± 4.7**	**348.1 ± 5.9**	**349.6 ± 3.3**	**344.5 ± 6.2**
RH_{lower}	%	r = 200–800 km	p = 850–700 hPa	**70.1 ± 7.3**	**68.8 ± 7.0**	**69.8 ± 5.6**	**64.2 ± 6.7**
RH_{middle}	%	r = 200–800 km	p = 700–500 hPa	**60.6 ± 10.7**	**56.9 ± 11.3**	**60.2 ± 7.7**	**49.8 ± 8.8**
RH_{upper}	%	r = 200–800 km	p = 500–300 hPa	**55.3 ± 11.7**	**50.5 ± 11.6**	**56.1 ± 7.6**	**42.9 ± 9.5**
Vorticity	10^{-7} s^{-1}	r = 0–1000 km	p = 850 hPa	30.3 ± 46.3	33.2 ± 52.9	**57.6 ± 45.0**	**9.7 ± 57.7**
Divergence	10^{-7} s^{-1}	r = 0–1000 km	p = 200 hPa	**43.2 ± 37.8**	**35.5 ± 33.4**	**81.1 ± 36.4**	**16.3 ± 39.7**

days, the mean and one standard deviation of IR brightness temperature values between 0 and 600 km over the entire day were calculated (Table 4, line 1). A Student's *t* test was used to determine if statistically significant differences were present at the 99% confidence level. Days with ACT pulses had overall colder IR brightness temperature values than days with INACT pulses, differences that were found to be statistically significant. This result was expected as ACT cooling pulses were associated with stronger amplitude diurnal pulses than INACT cooling pulses (Figs. 3, 4, and 7a,b) and ACT warming pulses were associated with highly convective off-the-clock cooling pulses (Figs. 3, 4, and 7e,f).

To determine whether the environment on ACT pulse days was more favorable for deep convection, the environments on ACT cooling-pulse and ACT warming-pulse days were compared to the environments during INACT cooling-pulse and INACT warming-pulse days by calculating the mean and standard deviation of SHIPS variables over the entire day (Table 4). A Student's *t* test at the 99% confidence level was again used to test significance.

Days that had ACT cooling pulses and ACT warming pulses had warmer SSTs, had higher OHC, and had more moist environments than their INACT day counterparts. These results indicate that days with ACT pulses had more thermodynamically favorable environments for deep convection. Additionally, for cooling- and warming-pulse days, ACT pulses had significantly higher upper-level divergence than INACT pulses. It is speculated that this difference is due to deeper convection in the ACT cooling pulse and in the off-the-clock cooling pulse associated with ACT warming pulses.

Days that had ACT cooling and warming pulses had a higher maximum potential intensity (MPI) than days with INACT cooling and warming pulses, where MPI is the theoretical upper bound in intensity of tropical cyclones, calculated by the thermodynamic disequilibrium between SST and upper-tropospheric temperature (Emanuel 1995). Since there was no statistical difference in intensity between ACT and INACT cooling-pulse days, this implies that days that had ACT cooling pulses were further from their MPI than INACT pulses. The same cannot be said for ACT and INACT warming pulses, since there was a statistical difference in the intensity between ACT and INACT warming-pulse days. Since the sample size of ACT warming pulses was very small (10 days), however, a larger sample is needed to conclude whether ACT warming pulses are further from their MPI than INACT warming pulses.

6. Conclusions

Ditchek et al. (2019) generated a climatology of Atlantic basin tropical cyclone diurnal pulses over a 36-yr period by creating an objective metric to identify diurnal pulses with similar temporal phasing as Dunion et al. (2014) using GridSat-B1 IR brightness temperature difference fields. That metric identified cooling pulses, similar to the pulses found in Dunion et al. (2014), and warming pulses, a previously unidentified pulse of warmer clouds propagating outward following the Dunion et al. (2014) clock. While Ditchek et al. (2019) provided a comprehensive analysis of the frequency and structure of diurnal pulses in the Atlantic basin, there were still many questions that remained unanswered, including how often diurnal pulses were convectively coupled. This study addressed that unanswered question by using WWLLN lightning data from 2005–17 to create an objective metric to identify pulses that were

electrically active and pulses that were electrically inactive based on lightning flash density, areal coverage, and longevity within a pulse.

Overall, cooling and warming pulses with electric activity occurred 61.1% of the time, with ACT pulses occurring 38.0% of the time and QUASI pulses occurring 23.1% of the time (Table 2). This left 38.9% of cooling- or warming-pulse days as INACT pulses.

The questions outlined in the introduction were answered for both ACT and INACT long-lived cooling- and warming-pulse days:

- Cooling pulses
  - Cooling pulses were ACT 43.9% of the time, were QUASI 24.1% of the time, and were INACT 32.0% of the time (Table 2).
  - Cooling pulses that were ACT had a larger percentage of pulses to the right of the shear vector in the preferred quadrants for enhanced outer-rainband lightning activity (Figs. 2a–f, 3, and 4).
  - ACT cooling pulses propagated outward more slowly than INACT cooling pulses, consistent with convectively coupled wave theory. Additionally, the increase of propagation speed with radius could imply that cold pool dynamics were occurring, supporting recent results that diurnal pulses may exhibit tropical squall-line-like characteristics (Figs. 7a–d).
  - Storms in lower-shear environments were more likely to have ACT and INACT cooling pulses (Figs. 8b).
  - ACT cooling-pulse days had oceanic and atmospheric environments that were more conducive to deep convection than INACT cooling-pulse days (Table 4).
- Warming pulses
  - Warming pulses were ACT 10.3% of the time, were QUASI 18.6% of the time, and were INACT 71.1% of the time (Table 2).
  - Warming pulses that were ACT had a slightly larger percentage of pulses to the right of the shear vector, in the preferred quadrants for enhanced outer-rainband lightning activity (Figs. 2g–l, 5, and 6).
  - ACT warming pulses had a slower outward propagation speed than INACT cooling pulses, consistent with convectively coupled wave theory. However, the INACT warming pulse had the slowest propagation speed, inconsistent with theory (Figs. 7e–h).
  - Warming pulses were more likely to occur in storms of weaker intensity. (Fig. 8a).
  - Storms in higher-shear environments were more likely to have ACT and INACT warming pulses (Fig. 8b).
  - ACT warming-pulse days had oceanic and atmospheric environments that were more conducive to deep convection than INACT warming-pulse days (Table 4).

Propagation speeds of ACT and INACT cooling pulses and ACT warming pulses lend support to the Dunion et al. (2019) result that pulses take on tropical squall-line characteristics after propagating away from the inner core as well as to the gravity wave interpretation of diurnal pulses.

On the other hand, since the INACT warming pulse was most certainly not associated with convection, the tropical squall-line interpretation does not apply to these pulses. Additionally, if INACT warming pulses were a nonconvectively coupled gravity wave, then according to convectively coupled wave theory, it should propagate outward faster than its convectively coupled wave counterparts (the ACT pulses and the INACT cooling pulse). It had the slowest propagation speed, however. Therefore, while the INACT warming pulse is still ''on the clock'', the gravity wave interpretation of diurnal pulses do not appear apply to INACT warming pulses. To understand the mechanism behind INACT warming pulses, case studies of INACT warming-pulse days should be conducted.

Acknowledgments. The authors thank reviewers Jason Dunion, Sarah Griffin, and John Knaff for their helpful comments about this research. GridSat-B1 IR brightness temperatures were acquired from NOAA's National Centers for Environmental Information (https://www.ncdc.noaa.gov/cdr/fundamental/geostationary-ir-channel-brightness-temperature-gridsat-b1). The authors also wish to thank the World Wide Lightning Location Network (http://wwlln.net), a collaboration among over 50 universities and institutions, for providing the lightning location data used in this paper. All authors were supported by NSF Grant AGS1636799.

REFERENCES

Abarca, S. F., K. L. Corbosiero, and T. J. Galarneau Jr., 2010: An evaluation of the Worldwide Lightning Location Network (WWLLN) using the National Lightning Detection Network (NLDN) as ground truth. *J. Geophys. Res.*, **115**, D18206, https://doi.org/10.1029/2009JD013411.

——, ——, and D. Vollaro, 2011: The World Wide Lightning Location Network and convective activity in tropical cyclones. *Mon. Wea. Rev.*, **139**, 175–191, https://doi.org/10.1175/2010MWR3383.1.

Black, R. A., and J. Hallett, 1999: Electrification of the hurricane. *J. Atmos. Sci.*, **56**, 2004–2028, https://doi.org/10.1175/1520-0469(1999)056<2004:EOTH>2.0.CO;2.

Browner, S. P., W. L. Woodley, and C. G. Griffith, 1977: Diurnal oscillation of the area of cloudiness associated with tropical storms. *Mon. Wea. Rev.*, **105**, 856–864, https://doi.org/10.1175/1520-0493(1977)105<0856:DOOTAO>2.0.CO;2.

Corbosiero, K. L., and J. Molinari, 2002: The effects of vertical wind shear on the distribution of convection in tropical cyclones. *Mon. Wea. Rev.*, **130**, 2110–2123, https://doi.org/10.1175/1520-0493(2002)130<2110:TEOVWS>2.0.CO;2.

——, and ——, 2003: The relationship between storm motion, vertical wind shear, and convective asymmetries in tropical cyclones. *J. Atmos. Sci.*, **60**, 366–376, https://doi.org/10.1175/1520-0469(2003)060<0366:TRBSMV>2.0.CO;2.

Deierling, W., and W. A. Petersen, 2008: Total lightning activity as an indicator of updraft characteristics. *J. Geophys. Res.*, **113**, D16210, https://doi.org/10.1029/2007JD009598.

DeMaria, M., and J. Kaplan, 1994: A Statistical Hurricane Intensity Prediction Scheme (SHIPS) for the Atlantic basin. *Wea. Forecasting*, **9**, 209–220, https://doi.org/10.1175/1520-0434(1994)009<0209:ASHIPS>2.0.CO;2.

——, and ——, 1999: An updated Statistical Hurricane Intensity Prediction Scheme (SHIPS) for the Atlantic and eastern North Pacific basins. *Wea. Forecasting*, **14**, 326–337, https://doi.org/10.1175/1520-0434(1999)014<0326:AUSHIP>2.0.CO;2.

——, M. Mainelli, L. K. Shay, J. A. Knaff, and J. Kaplan, 2005: Further improvements to the Statistical Hurricane Intensity Prediction Scheme (SHIPS). *Wea. Forecasting*, **20**, 531–543, https://doi.org/10.1175/WAF862.1.

——, R. T. DeMaria, J. A. Knaff, and D. Molenar, 2012: Tropical cyclone lightning and rapid intensity change. *Mon. Wea. Rev.*, **140**, 1828–1842, https://doi.org/10.1175/MWR-D-11-00236.1.

Dias, J., and O. Pauluis, 2009: Convectively coupled waves propagating along an equatorial ITCZ. *J. Atmos. Sci.*, **66**, 2237–2255, https://doi.org/10.1175/2009JAS3020.1.

Ditchek, S. D., J. Molinari, K. L. Corbosiero, and R. G. Fovell, 2019: An objective climatology of tropical cyclone diurnal pulses in the Atlantic basin. *Mon. Wea. Rev.*, **147**, 591–605, https://doi.org/10.1175/MWR-D-18-0368.1.

Dunion, J. P., C. D. Thorncroft, and C. S. Velden, 2014: The tropical cyclone diurnal cycle of mature hurricanes. *Mon. Wea. Rev.*, **142**, 3900–3919, https://doi.org/10.1175/MWR-D-13-00191.1.

——, ——, and D. S. Nolan, 2019: Tropical cyclone diurnal cycle signals in a hurricane nature run. *Mon. Wea. Rev.*, **147**, 363–388, https://doi.org/10.1175/MWR-D-18-0130.1.

Emanuel, K. A., 1995: Sensitivity of tropical cyclones to surface exchange coefficients and a revised steady-state model incorporating eye dynamics. *J. Atmos. Sci.*, **52**, 3969–3976, https://doi.org/10.1175/1520-0469(1995)052<3969:SOTCTS>2.0.CO;2.

Evans, R. C., and D. S. Nolan, 2019: Balanced and radiating wave responses to diurnal heating in tropical cyclone–like vortices using a linear nonhydrostatic model. *J. Atmos. Sci.*, **76**, 2575–2597, https://doi.org/10.1175/JAS-D-18-0361.1.

Knaff, J. A., C. J. Slocum, and K. D. Musgrave, 2019: Quantification and exploration of diurnal oscillations in tropical cyclones. *Mon. Wea. Rev.*, **147**, 2105–2121, https://doi.org/10.1175/MWR-D-18-0379.1.

Kossin, J. P., 2002: Daily hurricane variability inferred from goes infrared imagery. *Mon. Wea. Rev.*, **130**, 2260–2270, https://doi.org/10.1175/1520-0493(2002)130<2260:DHVIFG>2.0.CO;2.

Lajoie, F., and I. Butterworth, 1984: Oscillation of high-level cirrus and heavy precipitation around Australian region tropical cyclones. *Mon. Wea. Rev.*, **112**, 535–544, https://doi.org/10.1175/1520-0493(1984)112<0535:OOHLCA>2.0.CO;2.

Landsea, C. W., and J. L. Franklin, 2013: Atlantic hurricane database uncertainty and presentation of a new database format. *Mon. Wea. Rev.*, **141**, 3576–3592, https://doi.org/10.1175/MWR-D-12-00254.1.

Muramatsu, T., 1983: Diurnal variations of satellite-measured Tbb areal distribution and eye diameter of mature typhoons. *J. Meteor. Soc. Japan*, **61**, 77–90, https://doi.org/10.2151/jmsj1965.61.1_77.

Navarro, E. L., G. J. Hakim, and H. E. Willoughby, 2017: Balanced response of an axisymmetric tropical cyclone to periodic diurnal heating. *J. Atmos. Sci.*, **74**, 3325–3337, https://doi.org/10.1175/JAS-D-16-0279.1.

Nolan, D. S., R. Atlas, K. T. Bhatia, and L. R. Bucci, 2013: Development and validation of a hurricane nature run using the joint OSSE nature run and the WRF model. *J. Adv. Model. Earth Syst.*, **5**, 382–405, https://doi.org/10.1002/jame.20031.

O'Neill, M. E., D. Perez-Betancourt, and A. A. Wing, 2017: Accessible environments for diurnal-period waves in simulated tropical cyclones. *J. Atmos. Sci.*, **74**, 2489–2502, https://doi.org/10.1175/JAS-D-16-0294.1.

Rodger, C., J. Brundell, R. Holzworth, and E. Lay, 2009: Growing detection efficiency of the World Wide Lightning Location Network. *AIP Conf. Proc.*, **1118**, 15–20, https://doi.org/10.1063/1.3137706.

Ruppert, J. H., and M. E. O'Neill, 2019: Diurnal cloud and circulation changes in simulated tropical cyclones. *Geophys. Res. Lett.*, **46**, 502–511, https://doi.org/10.1029/2018GL081302.

Steranka, J., E. B. Rodgers, and R. C. Gentry, 1984: The diurnal variation of Atlantic Ocean tropical cyclone cloud distribution inferred from geostationary satellite infrared measurements. *Mon. Wea. Rev.*, **112**, 2338–2344, https://doi.org/10.1175/1520-0493(1984)112<2338:TDVOAO>2.0.CO;2.

Stevenson, S. N., K. L. Corbosiero, and S. F. Abarca, 2016: Lightning in eastern North Pacific tropical cyclones: A comparison to the North Atlantic. *Mon. Wea. Rev.*, **144**, 225–239, https://doi.org/10.1175/MWR-D-15-0276.1.

——, ——, M. DeMaria, and J. L. Vigh, 2018: A 10-year survey of tropical cyclone inner-core lightning bursts and their relationship to intensity change. *Wea. Forecasting*, **33**, 23–36, https://doi.org/10.1175/WAF-D-17-0096.1.

Wheeler, M., and G. N. Kiladis, 1999: Convectively coupled equatorial waves: Analysis of clouds and temperature in the wavenumber–frequency domain. *J. Atmos. Sci.*, **56**, 374–399, https://doi.org/10.1175/1520-0469(1999)056<0374:CCEWAO>2.0.CO;2.

Wu, Q., and Z. Ruan, 2016: Diurnal variations of the areas and temperatures in tropical cyclone clouds. *Quart. J. Roy. Meteor. Soc.*, **142**, 2788–2796, https://doi.org/10.1002/qj.2868.

Zipser, E. J., and K. R. Lutz, 1994: The vertical profile of radar reflectivity of convective cells: A strong indicator of storm intensity and lightning probability? *Mon. Wea. Rev.*, **122**, 1751–1759, https://doi.org/10.1175/1520-0493(1994)122<1751:TVPORR>2.0.CO;2.